ELECTRON CLOUD MEASUREMENTS AND SIMULATIONS FOR RHIC*

W. Fischer†, J.M. Brennan, M. Blaskiewicz, and T. Satogata
Brookhaven National Laboratory, Upton, NY 11973, USA

Abstract

Intense ion beams in RHIC lead to a rise in the vacuum pressure. Electron clouds can contribute to such a process. To measure electron cloud densities the coherent tune shift along the bunch train was observed with different bunch spacings and intensities. From the measured coherent tune shift electron cloud densities are computed and compared with densities obtained in electron cloud simulations.

1 INTRODUCTION

During the RHIC 2001 gold run the number of ions per bunch was continually increased up to the design value of 10^9 at the end of the run. Furthermore, it was attempted to double the number of bunches per ring from 55 to 110. Operation with 110 bunches led to pressure bumps with pressures high enough to prevent operation. In some instances the pressure in the warm sections increased from 10^{-9} Torr to 10^{-4} Torr [2]. With the design intensity of 10^9 ions per bunch and 55 bunches in each beam stored at injection, the vacuum system also aborted the beams. Basic machine parameters are listed in Tab. 1, a complete overview can be found in Ref. [1].

Measurements were initiated to characterize the electron cloud built-up and to investigate the possible role of electron clouds in the pressure rise. Since no dedicated electron detectors are currently available in RHIC these measurements were beam-based. To obtain an estimate of the electron cloud density, the coherent tune shift along the bunch train was determined. The estimated electron cloud densities can be compared with simulation results. Such comparisons were also done for the low energy ring of KEKB [3] and the SPS [4, 5].

The last RHIC run also allowed the measurement of proton beams. Gold and proton beams have the same number of bunches and approximately the same charge per bunch (see Tab. 1), but their interaction with the rest gas and the wall is different [6]. All tune shift measurements were performed at injection, where gold and proton beams have the same rigidity. The RHIC beam pipe is round almost everywhere. The average beta functions are the same for both planes, so are the beam emittances.

2 COHERENT TUNE SHIFT MEASUREMENTS

Coherent tunes shifts along bunch trains at injection were measured with two methods. First, a single beam position monitor (BPM) in each plane recorded the injection oscillations of the last incoming bunch. These BPMs are part of the tune meter system [7]. Typically 1024 turns were recorded and the tunes are obtained from a Fast Fourier Transform (FFT) of the coherent beam oscillations. An example is shown in Fig. 1. In this case 110 bunches were injected with an average intensity of $0.3 \cdot 10^{11}$ protons per bunch. The total tune shift after 110 bunches amounts to $2.5 \cdot 10^{-3}$. For gold beams and proton beams with large bunch spacing the resolution of these tune measurements was comparable to the tune shifts observed. The tune measurements were improved with a second method.

Table 1: Machine and beam parameters for gold and protons during RHIC Run 2001/2002, at injection.

parameter	unit	Au^{79+}	p^+
atomic number Z	...	79	1
mass number A	...	197	1
relativistic γ	...	10.5	25.9
harmonic no. h	...	360	360
no. of bunches	...	55/110	55/110
bunch spacing	ns	216/108	216/108
ions per bunch N_b	...	10^9	10^{11}
emitt. $\epsilon_{N\,x,y\,95\%}$	μm	10	25
bunch area $S_{95\%}$	eV·s/u	0.4	1.0
full bunch length	ns	18	14

The orbit system was set to record the injection oscillations of the last incoming bunch in 12 BPMs. In this measurement, all BPM data were filtered and the peak in the spectrum interpolated. In addition, the tune of each bunch

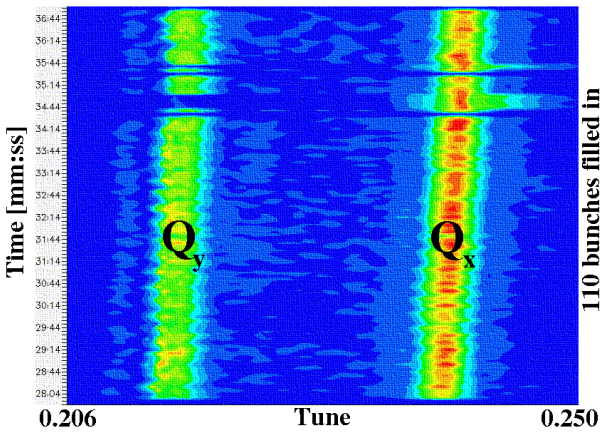

Figure 1: Coherent tunes measured along a Yellow train of 110 proton bunches with 105 ns spacing. Due to coupling both transverse tunes are visible.

* Work supported by US DOE under contract DE-AC02-98CH10886.
† Email: Wolfram.Fischer@bnl.gov

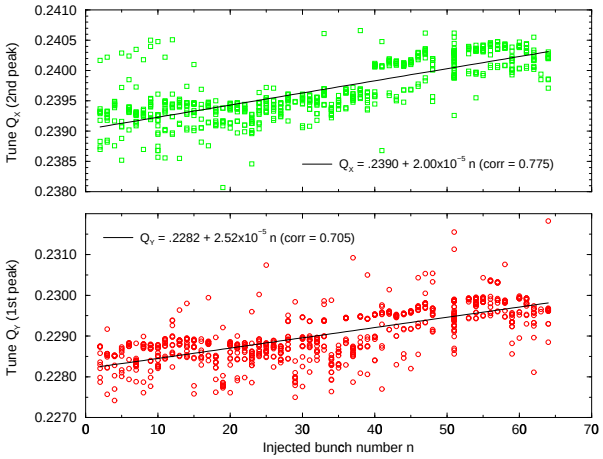

Figure 2: Coherent tunes measured along a Blue train of 63 gold bunches with 105 ns spacing. Individual dots correspond to the tunes from different BPMs. The solid lines are linear fits to the data.

could be obtained as an average of the 12 BPM measurements. This procedure is outside the current operational capabilities of the BPM system. A measurement is shown in Fig. 2. In this case a train of 63 bunches was injected with an average intensity $0.65 \cdot 10^9$ gold ions. The vacuum system aborted the fill. Furthermore, a transfer function measurement was tested from which the tunes along the bunch trains can be obtained.

In the measurements, an increase in both transverse tunes was observed, consistent with the existence of an electron cloud. The tune shift is about the same for the horizontal and vertical plane.

In Tab. 2 the results of all measurements are summarized. Measured tune shifts are of order 10^{-3} and are sometimes comparable to the measurement resolution. The data are consistent with the expectation that higher beam intensities and shorter bunch spacing lead to larger tune shifts.

3 ELECTRON CLOUD DENSITIES

A bunch passing each turn through a static electron cloud with uniform spatial density ρ_e experiences a coherent tune shift [8–10]

$$\Delta Q_{x,y} = \rho_e \left(\frac{r_p Z}{\gamma A} \right) \frac{h_{y,x} \beta_{x,y} L}{(h_x + h_y)}, \qquad (1)$$

where $h_{x,y}$ are the semi axes of an elliptical chamber, $\beta_{x,y}$ the average beta functions, L the length of the sections with electron clouds, and $r_p = 1.5347 \cdot 10^{-18}$ m the classical proton radius. In the case of a round beam chamber ($h_x = h_y = h$) and round beams ($\beta_x = \beta_y = \beta$) the tune shifts in both planes are the same ($\Delta Q_x = \Delta Q_y = \Delta Q$) and Eq. (1) can be simplified to

$$\Delta Q = \rho_e \left(\frac{r_p Z}{\gamma A} \right) \frac{\beta L}{2}. \qquad (2)$$

Table 2: Measured coherent tune shifts ΔQ along bunch trains. The values given are the difference in tune between bunch 55 and bunch 1, and are averaged over the horizontal and vertical tune shift. The number of measurements is shown in brackets.

bunch spacing	charge per bunch	tune shift ΔQ	
		Au^{79+}	p^+
[ns]	$[10^{10} e]$	$[10^{-3}]$	$[10^{-3}]$
216	7.6	1.1 (2)	–
216	8.7	–	0.3 (12)
108	3.0	–	1.3 (2)
108	5.4	1.1 (4)	–

Assuming that the electron cloud fills the whole beam pipe, the electron line density is $\lambda_e = \pi r^2 \rho_e$ where r denotes the average beam pipe inner radius. The charge line density is given by $\lambda_{ce} = \lambda_e e$ where e is the electron charge.

We consider the cases of electron clouds in the whole ring and clouds in the warm regions only. The latter is motivated by the fact that significant pressure rises were only observed in warm region.

For relativistic ion beams with the same rigidity the factor $(r_p Z/\gamma A)$ in Eq. (2) is approximately constant. However, gold and proton beams were injected into different lattices, resulting in different values for β in both cases.

The relevant machine parameters for all cases and the computed electron cloud densities are shown in Tab. 3. With the assumptions made, one expects charge line densities of 0.2 to 2 nC/m to account for the measured tune shifts.

Eq. (2) gives only a rough estimate for the electron cloud density for two reasons. First, with long bunches the cloud may not be static while the bunch is passing through. In RHIC electrons can perform a few oscillations during a bunch passage. Second, the cloud density may not be distributed uniformly in space. In Ref. [10] the effect of

Table 3: Machine parameters and computed electron cloud densities for different cloud lengths and species.

parameter	unit	Au^{79+}	p^+
tune shift ΔQ	10^{-3}	1.1	1.3
r whole ring	m	0.04	
r warm regions only	m	0.06	
β whole ring	m	30	36
β warm regions only	m	42	76
L whole ring	m	3834	
L warm regions only	m	700	
ρ_e whole ring	10^{11} m^{-3}	3.3	2.9
ρ_e warm regions only	10^{11} m^{-3}	12.8	7.6
λ_e whole ring	10^9 m^{-1}	1.6	1.4
λ_e warm regions only	10^9 m^{-1}	14.5	8.6
λ_{ce} whole ring	nC·m^{-1}	0.26	0.22
λ_{ce} warm regions only	nC·m^{-1}	2.32	1.38

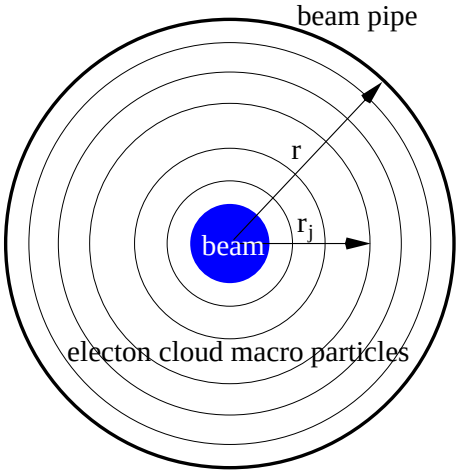

Figure 3: Geometry used in the electron cloud simulations.

the bunch length on the observed tune shift is investigated analytically and numerically. Significant deviations from Eq. (2) are found for electron clouds of size comparable to the beam size while the equation holds for electron clouds large compared to the beam size. In the simulations reported in Sec. 5 it is found that the electron cloud is much larger than the beam size. This was also found in a RHIC simulation with another code [11]. A transversely large electron cloud, filling most of the beam pipe, is also a good approximation for a cloud with uniform spatial density. Thus Eq. (2) should give a useful estimate for the electron cloud densities.

4 ELECTRON CLOUD SIMULATIONS

The computer code used here was written by one of the authors (M.B.) to study both the effects of electron gap survival and the electric fields generated by the electrons [12]. It was used previously for the PSR [13] and the SNS [14].

The code assumes that the positively charged ion beam and the electron cloud are both cylindrically symmetric within a round, straight vacuum chamber, without an external magnetic field. Longitudinal electric fields are ignored, since they produce velocities small compared to the beam velocity. The spatial distribution of the electron cloud is modeled as a sum of N_{macro} cylindrical shells which serve as macro particles. This is shown in Fig. 3. The macro particle shells can have an angular momentum.

The evolution of the cloud is computed by accelerating the shells, and creating secondary electrons when the macro particles hit the wall. In addition, electrons are created either at the wall or in the beam pipe with a generation rate proportional to the instantaneous beam line density. The generation rate must be estimated outside the program from processes such as rest gas ionization or beam loss driven electron generation.

The acceleration of shell j, with radius r_j, due to shell k, with radius r_k is taken to be nonzero only if $r_j > r_k$. In this case the acceleration is

$$\ddot{r}_j = 2r_e c^2 \lambda_k \frac{r_j}{d^2 + r_j^2}, \tag{3}$$

where r_e is the classical electron radius, c the speed of light and λ_k is the electron line density of shell k. The smoothing length d is typically an order of magnitude smaller than the beam size. The electric field due to the ion beam has the same form as that due to electrons at $r = 0$, λ_e being replaced by the instantaneous beam line density multiplied by the ion charge state, $Z\lambda_b$.

The time dependence of the instantaneous beam line density is given by

$$\lambda_b(t) = \lambda_{b,peak}\left(1 - \frac{t^2}{\tau^2}\right)^n, \tag{4}$$

where n can be chosen to fit the measured longitudinal beam profile. For large n formula (4) approximates a Gaussian beam profile. τ is a measure for the beam length.

The beam is typically divided into several thousand longitudinal slices N_{slice}, and the electron cloud is updated with every longitudinal slice. Electron macro particles can carry different charges with a minimum and maximum charge defined. Macro particle numbers range from hundreds to hundreds of thousands.

The generation of secondary electrons follows largely a model that is presented in Ref. [15]. When an electron macro particle with energy E hits the wall, it is first determined whether the electron is reflected or generates secondary electrons. In the following, x_r denotes a random number out of a uniform distribution between zero and one. The electron is reflected if

$$x_{r1} < P_\infty + (P_0 - P_\infty)e^{-E/E_{\text{reflect}}}, \tag{5}$$

where P_0, P_∞, and E_{reflect} are input parameters that should be determined in measurements. P_0 and P_∞ are the probabilities of reflection at zero and large energy respectively.

If the electron macro particle is reflected, it can be reflected elastically or it can be rediffused. It is rediffused if

$$x_{r2} < P_{\text{rediffuse}}, \tag{6}$$

where $P_{\text{rediffuse}}$ is an input parameter. Otherwise it is elastically reflected. In the former case the energy of the outgoing electron macro particle is $x_{r3}E$; in the latter case it is E.

If the electron macro particle is not reflected, it generates secondary electron macro particles with the emission yield δ given by

$$\delta(E) = \delta_{max} \times 1.1\left(\frac{1 - \exp\left[-2.3(E/E_{max})^{1.35}\right]}{(E/E_{max})^{0.35}}\right). \tag{7}$$

δ_{max} and E_{max} are input parameters. The line density of the generated macro particle is

$$\lambda_{k,out} = \lambda_k \delta(E) e^{\alpha_\delta(1-\cos\theta)}, \tag{8}$$

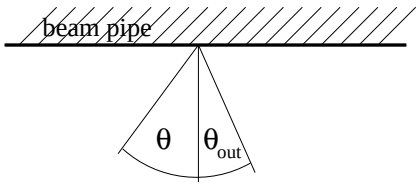

Figure 4: Definition of angle θ.

where α_δ is an input parameter and θ is the incident angle relative to the surface normal (see Fig. 4). If the line density is below the set limit, the macro particle is dropped. If the line density is above the set limit, more than one macro particle is generated. The energy of the generated macro particles is

$$E_{out} = E_{\mathrm{secondary}} \tan\left(\frac{\pi}{2} x_{r4}\right). \qquad (9)$$

$E_{\mathrm{secondary}}$ is an input parameter.

The distribution of the output angle θ_{out} is the same for reflected and secondary electrons, and independent of the incident angle θ, thus assuming a rough surface. The distribution of θ_{out} is given by

$$P(\theta)\, d\theta \propto (\cos\theta)^{\alpha_\theta} \sin\theta\, d\theta, \qquad (10)$$

where the parameter α_θ is an input parameter between zero (equivalent to black body radiation) and infinity ($\theta_{out} = \mathrm{const} = \pi/2$). The list of input parameters is shown in Tab. 4.

5 SIMULATION RESULTS

Since the simulations have many input parameters and the result is very sensitive to changes in a number of those we first define reference cases for gold and proton beams. The reference cases should be close to worst case scenarios with respect to the beam parameters. We will then vary input parameter in one of the reference cases to find the sensitivity of the result with respect to these parameters.

The two reference cases are based on design intensities and short bunch spacing. The cases differ slightly in the charge per bunch and significantly in the bunch length. Furthermore, rest gas ionization is assumed for the proton case and loss-driven electron generation in the gold case. Beam and beam pipe sizes correspond to an assumed electron cloud in the whole machine. The two cases are listed in Tab. 4.

In Figs. 5-10 the simulation output is shown for the proton reference case. Fig. 5 shows the ion beam and electron cloud charge line densities. After 25 bunches the electron cloud is saturated at approximately 0.3 nC/m. The saturation is also visible in Fig. 8 which only shows the last three bunches. The saturation charge line density is comparable to expectations from the tune shift measurements (cf. Tab. 3). However, the tune shift measurements were done at lower bunch charges.

Table 4: List of input parameters for electron cloud simulations. For gold and proton beams reference cases are presented with design intensity and twice the design bunch number.

parameter	unit	Au^{79+}	p^+
bunch spacing	ns	108	
bunches	...	55	
rms beam radius	mm	2.2	2.4
pipe radius	mm	40	
electrons generated/bunch	...	40000	100
electron generation radius	mm	40	2.4
full bunch length	ns	18	14
bunch shape parameter n	...	3	3
bunch charge	nC	13	16
longitudinal slices	...	5000	
macro particles, initially	...	2500	250
smoothing length d	mm	0.1	
λ_{ce}, initial	$\mathrm{pC{\cdot}m^{-1}}$	1.6	
P_0	...	0.8	
P_∞	...	0.2	
E_{reflect}	eV	60	
$P_{\mathrm{rediffuse}}$	...	0.5	
δ_{max}	...	2.5	
E_{max}	eV	300	
$E_{\mathrm{secondary}}$	eV	20	
α_δ	...	0.5	
α_θ	...	1.0	

Figs. 6 and 9 show the transverse rms size of the ion beam and electron cloud for the whole bunch train and the last three bunches respectively. The electron cloud size drops while the second half of the bunch is passing, as accelerated electrons hit the wall. On average the electron cloud is much larger than the ion beam and its rms size is consistent with a approximately uniform density. For a transverse uniformly distributed electron cloud, the rms size would be $r/\sqrt{2}$.

In Figs. 7 and 10 the average kinetic energy of the electrons and the electron current into the wall are shown. From this, an estimate of the heat load into the wall can be obtained. From Fig. 10 one finds an average kinetic energy of approximately 0.03 keV and average electron current of about 20 mA/m. This corresponds to a heat load of 0.6 W/m or 1.8 kW for the cold part of the ring, assuming that all kinetic energy is transformed into heat. No increased heat load was observed during the tests in 2001. The minimum detectable heat load is 150W [16].

The simulation of the gold beam reference case shows no significant increase in the initial electron line density. The final density after 55 bunches is two orders of magnitude smaller than in the proton reference case. This is largely due to the longer bunches and the reduced charge per bunch.

The sensitivity of the computed electron cloud density with respect to the input parameters was estimated by varying single input parameters only. This is shown in Tab. 5.

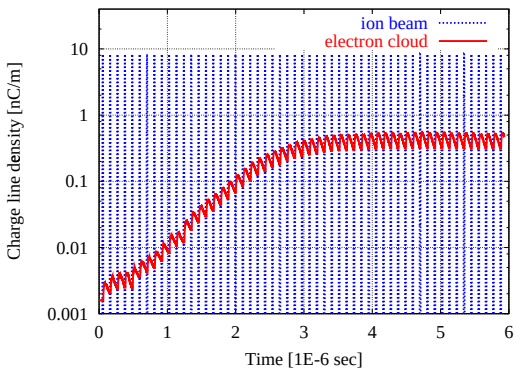

Figure 5: Ion beam and electron cloud line density for the proton reference case.

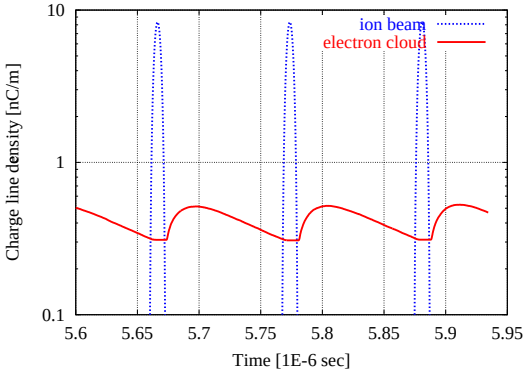

Figure 8: Ion beam and electron cloud line density for the last three bunches of the proton reference case.

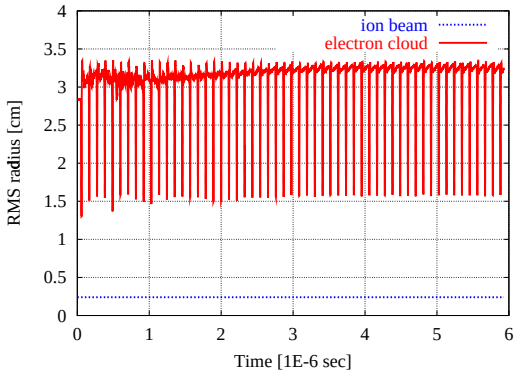

Figure 6: Ion beam and electron cloud transverse rms sizes for the proton reference case.

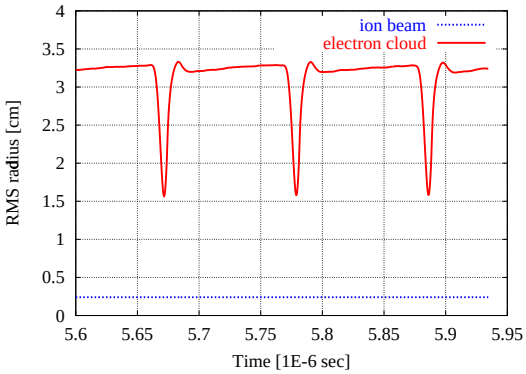

Figure 9: Ion beam and electron cloud transverse rms sizes for the last three bunches of the proton reference case.

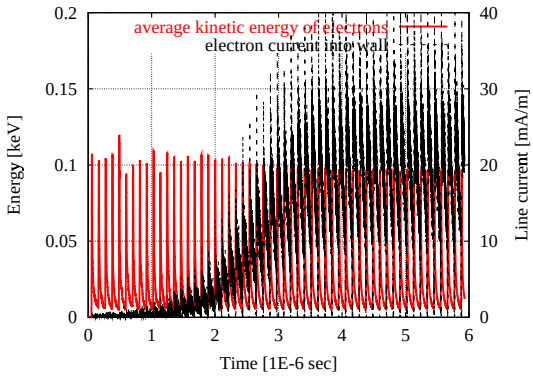

Figure 7: Average kinetic energy of electrons and electron current into the beam pipe wall for the proton reference case.

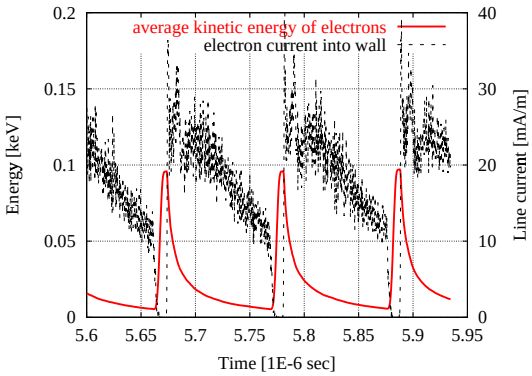

Figure 10: Average kinetic of electrons and current into the beam pipe wall for the last three bunches of the proton reference case.

Table 5: Maximum charge line density after 55 bunches in simulations under variation of input parameters. In each case only one parameter of the proton reference case is changed and the resulting line density is shown together with its relative change.

parameter	unit	value	change [%]	λ_{ce} [nC/m]
(ref. case p)	...	...	...	**0.5**
bunch spacing	ns	216	$+100$	0.00
beam radius	mm	4.8	$+100$	0.4
pipe radius	mm	60	$+50$	0.02
e-gen./bunch	...	50	-50	0.5
e-gen./bunch	...	1000	$+1000$	0.5
e-gen. radius	mm	40	$+1660$	0.5
bunch length	ns	18	$+28$	0.4
bunch length	ns	10	-28	0.6
bunch shape n	...	1	...	0.3
bunch shape n	...	6	...	0.6
bunch charge	nC	12	-25	0.00
bunch charge	nC	14	-12	0.2
bunch charge	nC	18	$+12$	0.8
N_{slices}	...	10000	$+200$	0.5
N_{macro}, initial	...	2500	$+1000$	0.5
smoothing d	mm	0.01	-90	0.5
λ_{ce}, initial	pC/m	0.016	-99	0.5
P_0	...	0.7	-12	0.2
P_∞	...	0.1	-50	0.5
E_{reflect}	eV	80	$+33$	0.6
$P_{\mathrm{rediffuse}}$	...	0.4	-20	0.6
δ_{max}	...	2.0	-20	0.00
δ_{max}	...	2.2	-12	0.01
E_{max}	eV	350	$+17$	0.1
$E_{\mathrm{secondary}}$	eV	30	$+50$	0.9
α_δ	...	0.4	-20	0.4
α_θ	...	0.0	-100	0.3
α_θ	...	5.0	$+500$	0.9

The simulation result is not sensitive to the number or location of electrons generated during a bunch passage, the number of longitudinal slices, the number of initial macro particles or the smoothing length d. It is also not sensitive to the initial line electron line density so that the final line density is determined through the parameters of the multiplication process. However, the result is, to a varying degree, sensitive to almost all other parameters.

6 SUMMARY

The signs of the measured coherent horizontal and vertical tune shifts along bunch trains in RHIC are consistent with the existence of electron clouds. From the measured tune shifts electron cloud densities were estimated. Electron cloud densities of the same order of magnitude could also be obtained in simulations with beam intensities somewhat higher than in the measurements. The cloud densities estimated from the tune shift measurements could not be reproduced with the bunch intensities in the measurement. Thus, physical effects may be missing in the simulation or there is an insufficient knowledge of the surface parameters.

7 ACKNOWLEDGMENTS

The authors would like to thank for support and discussions: M. Bai, P. Cameron, M.A. Furman, M. Harrison, H.C. Hseuh, T. Kerner, W. MacKay, T. Nicoletti, F. Pilat, M. Pivi, T. Roser, W.C. Turner, S. Tepikian, D. Trbojevic, S.Y. Zhang, and F. Zimmermann.

8 REFERENCES

[1] H. Hahn (editor), "RHIC design manual", revision of October 2000, http://www.rhichome.bnl.gov/NT-share/rhicdm/00_toc1i.htm.

[2] S.Y. Zhang, "RHIC vacuum pressure bump", BNL C-A/AP/67 (2002).

[3] G. Rumolo, F. Zimmermann, H. Fukuma, and K. Ohmi, "Electron cloud studies for KEKB", proceedings of the 2001 Particle Accelerator Conference, Chicago (2001).

[4] G. Arduini, K. Cornelis, G. Ferioli, L. Jensen, and F. Zimmermann, "Transverse instabilities of the LHC proton beam in the SPS", proceedings of the 2000 European Particle Accelerator Conference, Vienna (2001).

[5] G. Arduini, K. Cornelis, W. Höfle, G. Rumolo, and F. Zimmermann, "Transverse behavior of the LHC proton beam in the SPS: an update", proceedings of the 2001 Particle Accelerator Conference, Chicago (2001).

[6] W. Fischer et al., "Vacuum pressure rise with intense ion beams in RHIC", to be published in the proceedings of the 2002 European Particle Accelerator Conference, Paris (2002).

[7] P. Cameron, R. Connolly, A. Drees, T. Ryan, H. Schmickler, T. Shea, and D. Trbojevic, " ARTUS: A Rhic TUne monitor System", BNL RHIC/AP/155 (1998).

[8] M.A. Furman and A.A. Zholents, "Incoherent effects driven by the electron cloud", proceedings of the 1999 Particle Accelerator Conference, New York (1999).

[9] F. Zimmermann, "The electron cloud instability: summary of measurements and understanding", proceedings of the 2001 Particle Accelerator Conference, Chicago (2001).

[10] K. Ohmi, S. Heifets, and F. Zimmermann, "Study of coherent tune shift caused by electron cloud in positron storage rings", proceedings of the 2001 Asian Particle Accelerator Conference, Beijing; CERN SL-2001-062 (AP) (2001).

[11] M.A. Furman, private communication (2001).

[12] M. Blaskiewicz, computer program csec (2001).

[13] M. Blaskiewicz et al, these proceedings (2002).

[14] V. Danilov, A. Aleksandrov, M. Blaskiewicz, and J. Wei, "Calculations of electron accumulation in the SNS storage ring", proceedings of the 2001 Particle Accelerator Conference, Chicago (2001).

[15] M.A. Furman and M. Pivi, "Microscopic probabilistic model for the simulation of secondary electron emission", LBNL-49711, CBP Note-415 (2002).

[16] T. Nicoletti, private communication (2001).